



KW-Sun: The Konus-Wind Solar Flare Database in Hard X-Ray and Soft Gamma-Ray Ranges

A. L. Lysenko¹ , M. V. Ulanov¹ , A. A. Kuznetsov² , G. D. Fleishman³ , D. D. Frederiks¹ , L. K. Kashapova² ,
Z. Ya. Sokolova¹ , D. S. Svinkin¹ , and A. E. Tsvetkova¹

¹ Ioffe Institute, Polytekhnicheskaya, 26, St. Petersburg, 194021, Russia; alexandra.lysenko@mail.ioffe.ru

² Institute of Solar-Terrestrial Physics (ISZF), Lermontov St., 126a, Irkutsk, 664033, Russia

³ New Jersey Institute of Technology, University Heights, Newark, NJ 07102-1982, USA

Received 2022 July 6; revised 2022 August 18; accepted 2022 August 19; published 2022 September 15

Abstract

We present a database of solar flares registered by the Konus-Wind instrument during more than 27 yr of operation, from 1994 November to now (2022 June). The constantly updated database (hereafter KW-Sun) contains over 1000 events detected in the instrument's triggered mode and is accessible online at <http://www.ioffe.ru/LEA/kwsun/>. For each flare, the database provides time-resolved energy spectra in energy range from ~ 20 keV to ~ 15 MeV in FITS format along with count-rate light curves in three wide-energy bands, G1 (~ 20 –80 keV), G2 (~ 80 –300 keV), and G3 (~ 300 –1200 keV), with high time resolution (down to 16 ms) in ASCII and IDL SAV formats. This article focuses on the instrument capabilities in the context of solar observations, the structure of the KW-Sun data, and their intended usage. The presented homogeneous data set obtained in the broad energy range with high temporal resolution during more than two full solar cycles is beneficial for both statistical and case studies as well as a source of context data for solar flare research.

Unified Astronomy Thesaurus concepts: [Solar flare spectra \(1982\)](#); [Solar flares \(1496\)](#); [Solar electromagnetic emission \(1490\)](#); [Solar gamma-ray emission \(1497\)](#); [Solar x-ray emission \(1536\)](#); [Solar x-ray flares \(1816\)](#)

1. Introduction

Hard X-ray (HXR) and gamma-ray emissions play a primary role in the diagnostics of electron and ion acceleration in solar flares. They provide information about the spectrum, energetics, and abundances of accelerated particles along with acceleration timescales (Fletcher et al. 2011). Therefore hard X-ray/gamma-ray data with high temporal and energy resolutions are of particular interest. The main mechanism responsible for HXR emission of solar flares is the bremsstrahlung emission of accelerated electrons (see, e.g., Holman et al. 2011, and references therein). Protons and heavier ions accelerated during a flare produce gamma-ray lines and a continuum due to numerous nuclear reactions (see, e.g., Vilmer et al. 2011, and references therein).

Spectral, temporal, and spatial characteristics of HXR and gamma-ray emission in solar flares are very diverse. The range of flare energies emitted in HXR and gamma-ray ranges extends over many orders of magnitude, from $\sim 10^{26}$ (Crosby et al. 1993) to $\sim 10^{32}$ erg for large eruptive flares (Emslie et al. 2012). Energy spectra of the so-called microflares (see, e.g., Hannah et al. 2008) barely reach 10 keV, the majority of solar flares demonstrate emission up to several tens of keV, and in some flares the spectra extend to GeV energies (see, e.g., Vestrand et al. 1999; Share et al. 2018). The flare durations range from a fraction of a second for short impulsive bursts to hours for gradual flares (Dennis 1985; Crosby et al. 1993).

Despite several decades of research, many questions in solar flare physics are still under discussion and require further development of instrumentation and theory (Fletcher et al.

2011). Among these questions are the particular mechanism (mechanisms) responsible for particle acceleration during reconnection, the cause of energy partitioning between different flare components including cases of 100% efficiency of the electron acceleration (Fleishman et al. 2022), and whether the same acceleration mechanism is involved in both short and long-duration HXR bursts, etc.

Due to the opacity of the Earth's atmosphere to X-rays and gamma-rays, the solar observations in these ranges became possible only with the beginning of exoatmospheric astronomy. Important results were obtained by low-Earth-orbit space observatories, among them OSO-5 (1969–1983), OSO-7 (1971–1974), Hinotori (1981–1991), the Solar Maximum Mission (1980–1989), Yokoh (Ogawara et al. 1991, Acton et al. 1992; 1991–2001), and RHESSI (Lin et al. 2002, 2002–2018). Since 1975 space telescopes on board the Geostationary Operational Environmental Satellite (GOES) spacecraft series continuously monitor solar soft X-ray emission in two broad energy channels providing the commonly accepted X-ray classification of solar flares (classes A, B, C, M, and X) according to their power. In 2020 February, Solar Orbiter (SolO, Müller et al. 2020) was launched into a heliocentric orbit with the purpose of investigating solar and heliospheric physics using a payload of instruments designed for both remote and in situ sensing. Among them is the Spectrometer/Telescope for Imaging X-rays (STIX, Krucker et al. 2020), which allows solar imaging in a 4–150 keV range from an off-ecliptical position. Although now there are no solar-dedicated HXR and gamma-ray instruments operating in near-Earth space, several high-energy detectors provide solar spectra and light curves in these ranges; e.g., Fermi-GBM (Meehan et al. 2009) and Fermi-LAT (Atwood et al. 2009; Ajello et al. 2021) at low-Earth orbit, which have operated since 2008, and Konus-Wind (Aptekar et al. 1995), which was launched in 1994 and operates in interplanetary space. Solar



Original content from this work may be used under the terms of the [Creative Commons Attribution 4.0 licence](#). Any further distribution of this work must maintain attribution to the author(s) and the title of the work, journal citation and DOI.

data from these instruments are freely accessible via the SolarSoft package,⁴ Virtual Solar Observatory,⁵ Interactive Multi-Instrument Database of Solar Flares and Heliportal,⁶ and other resources.

Here we present KW-Sun, a database of Konus-Wind solar flare observations that cover more than two full solar cycles, from 1994 to the present. The main objectives of Konus-Wind are the studies of high-energy transient emission from distant astrophysical sources, such as cosmological gamma-ray bursts and soft gamma-repeater (magnetar) flares. Although the systematic use of the Konus-Wind data for solar physics applications began only recently, it has already yielded important results (see a review by Lysenko et al. 2020). The KW-Sun database has been developing since 2016, and many improvements in data analysis and presentation have been made over the past few years.

Konus-Wind has a number of advantages for solar flare studies compared to other instruments. These include: a high temporal resolution in the triggered mode, which allows one to reconstruct accelerated electron properties and obtain constraints on the acceleration mechanism (Glesener & Fleishman 2018; Altyntsev et al. 2019); a wide-energy range that covers emission from accelerated electrons and a good fraction of emission from nuclear reactions of accelerated ions (e.g., Lysenko et al. 2019 and references therein); and last but not least the instrument location in interplanetary space that allows for observations of the Sun in stable background conditions for $\gtrsim 90\%$ of the time.

2. Konus-Wind

The Konus-Wind spectrometer was launched on board the NASA Wind spacecraft in 1994 November and has operated until the present day (Wilson et al. 2021). Wind is a spin-stabilized spacecraft with a spin axis aligned with ecliptic south and a spin period of ~ 3 s.⁷ Since 2004 July, the spacecraft has been in orbit around Lagrange point L1 at ~ 5 lt-s from the Earth. Operating in interplanetary space the instrument sees the Sun 24 hr a day and being far from the Earth's radiation belts it has an exceptionally stable background. The total fraction of time when the Konus-Wind data are unavailable or contaminated by a high-solar-particle background does not exceed 10%.⁸

Konus-Wind consists of two cylindrical NaI(Tl) detectors, S1 and S2, mounted on the opposite sides of the rotationally stabilized spacecraft so that they point to the southern and the northern ecliptic poles, respectively. Consequently, the solar emission enters the detectors from the lateral side, at an incident angle of $(90 \pm 1)^\circ$ to the axis, and is registered in both S1 and S2 (Figure 1). Due to Wind's rotation, Konus-Wind suffers from occultations from other instruments and spacecraft structures that is important for studies of solar flare time histories on millisecond timescales (see details in Section 3.1).

The instrument operates in two modes: waiting and triggered. In the waiting mode, the count rates in three wide-

energy bands, G1 (~ 20 – 80 keV), G2 (~ 80 – 300 keV), and G3 (~ 300 – 1200 keV), are available with a time resolution of 2.944 s along with the count rate at energies $\gtrsim 10$ MeV (the Z channel). As the gamma-ray flux at the higher energies is low compared to the charged particle background, the Z-channel data can be used to monitor flux variations of high-energy electrons and ions.

When the count rate in G2 exceeds a $\sim 9\sigma$ threshold above the background on one of two fixed timescales, 1 s or 140 ms, the instrument switches into the triggered mode. Thus, rather spiky and spectrally hard (with a significant emission above ~ 80 keV) flares are recorded in the triggered mode, while more gradual and soft events are typically registered in the waiting mode only.

In the triggered mode, the count-rate curves in G1, G2, and G3 are recorded with a high time resolution during an interval of 229 s. The time resolution constitutes 2 ms for the time period from 0.512 s before the trigger to 0.512 s after the trigger time, 16 ms from 0.512 to 33.280 s after the trigger, 64 ms from 33.280 to 98.816 s after the trigger, and 256 ms for the remaining triggered-time history. In the KW-Sun database we merge adjacent 2 ms bins into 16 ms bins. Along with the high-resolution triggered-mode light curves, the waiting-mode record continues until ~ 250 s after the trigger time.

Starting from the trigger time, 64 energy spectra are accumulated, over pseudologarithmic energy scales, in two partially overlapping energy ranges, PHA1 (63 channels, ~ 20 – 1200 keV) and PHA2 (60 channels, ~ 0.35 – 15 MeV). For the first four spectra the accumulation time is fixed at 64 ms and for the last eight spectra at 8.192 s. For spectra from 5 to 56, the accumulation time varies between 256 ms and 8.192 s according to the count rate in G2: with the intensity increase the accumulation time decreases. Thus, the spectra may cover a time interval with a total duration varying from 79.104 s for very bright flares to 492 s for less intense events. After the end of the trigger record, the measurements are stopped for ~ 1 hr due to the data readout, and only the count rate in G2 is available with the time resolution of 3.68 s.

As the triggered-mode record is limited in time (~ 250 s for the time profiles and ≤ 492 s for multichannel spectra) the record can stop before the actual end of the flare for long-duration events.

For each flare, the instrument energy scale is calibrated using the 1460 keV line of ^{40}K . Temporal evolutions of energy boundaries for S1 and S2 are shown in Figure 2.

The energy resolution ($\text{FWHM}/E = \Delta E/E$) of Konus-Wind depends on energy and constitutes $\sim 20\%$ at 20 keV and $\sim 5\%$ at 2 MeV. The spectral resolution of the detectors did not change significantly during the mission, and the corresponding resolution loss is less than a factor of 1.5 as compared to the ground-based calibrations (Svinkin et al. 2016).

For most flares, a standard Konus-Wind dead-time (DT) correction procedure (i.e., a simple nonparalyzable DT correction in each of the measurement bands, with a DT of a few microseconds for light curves and $\sim 42 \mu\text{s}$ for multichannel spectra) provides a robust flux estimate. Details of DT corrections for very intense flares are given in Section 3.3.2.

3. KW-Sun Database

By the time of writing, 2022 June, Konus-Wind registered $\sim 13,000$ solar flares in the waiting mode, 1065 flares in the triggered mode, and, among them, 93 flares with emission at

⁴ <https://www.lmsal.com/solarsoft/>

⁵ <https://sdac.virtualsolar.org/cgi/search>

⁶ <https://Sun.njit.edu/About/IMIDSFH.html>

⁷ The deviation of the spacecraft's spin axis from the ecliptic north–south axis does not exceed 1° and the spin period varies gradually in the interval of 3.0–3.2 s.

⁸ Detailed information on the availability of Konus-Wind data for a particular time can be obtained from the authors on request.

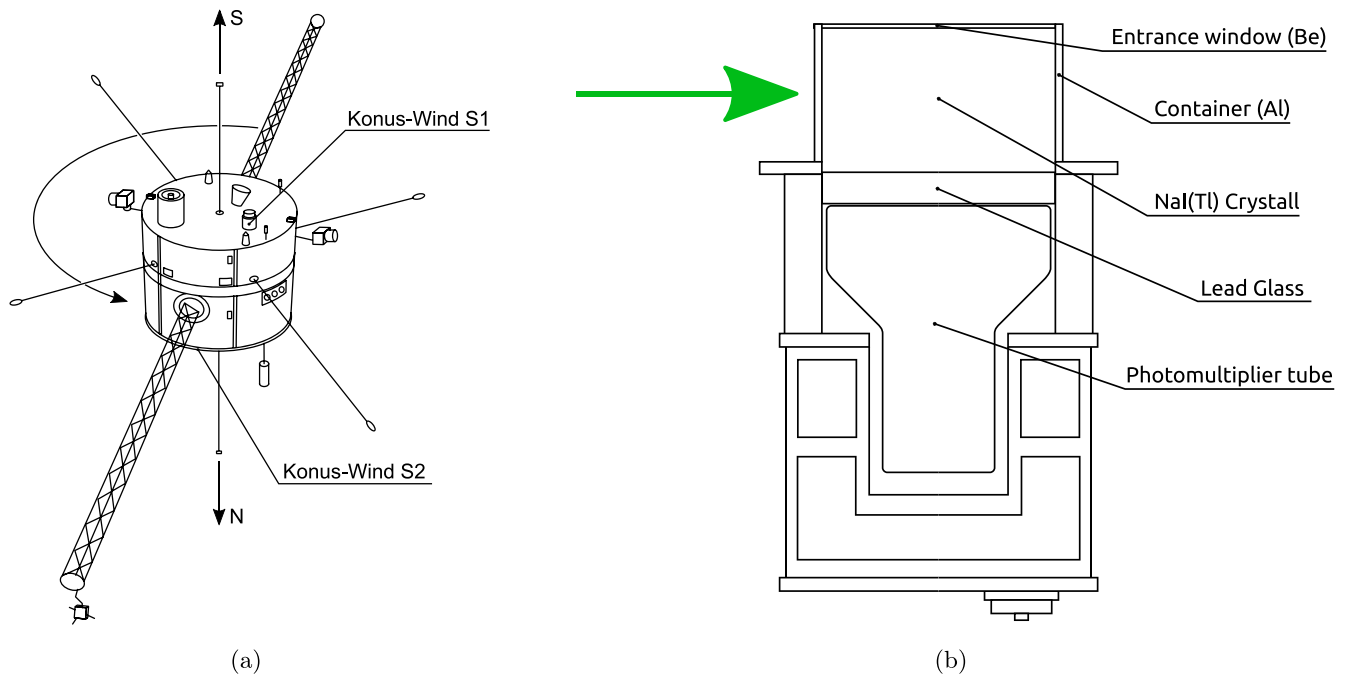


Figure 1. Konus-Wind: (a) the location of Konus detectors S1 and S2 on the spacecraft, “N” and “S” are the directions to the ecliptic poles and the circular arrow indicates the spin direction of the spacecraft; (b) a scheme of the Konus detector. The green arrow indicates the direction of solar emission.

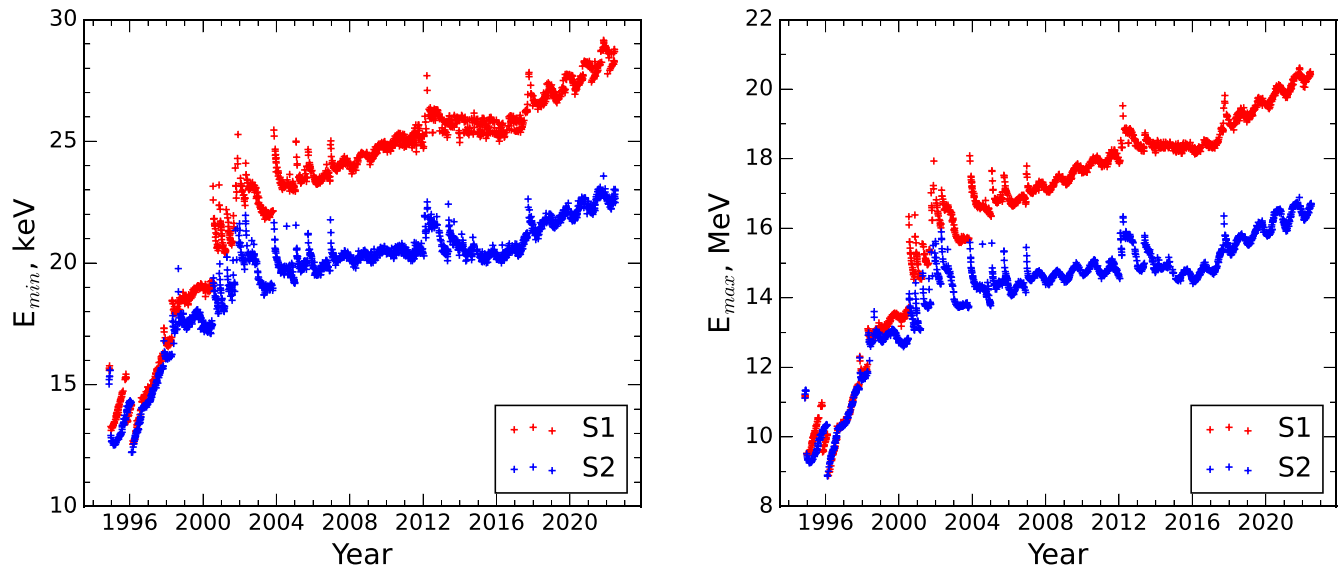


Figure 2. Temporal evolutions of Konus-Wind low-energy boundaries (left) and high-energy boundaries (right) for detectors S1 and S2.

high, >1 MeV, energies. Annual statistics of the triggered solar flares categorized according to their GOES classes are presented in Figure 3.

To identify a detected event as a solar flare we check if (i) the net count rates in both Konus detectors are close to each other, and (ii) there is a corresponding flare in the GOES event list⁹ or a simultaneous flux increase in the GOES soft X-ray sensor data in the 1–8 Å and 0.5–4.0 Å bands. In controversial cases, we analyze spatial information from other telescopes.

As Konus-Wind does not have an anticoincidence shield to filter out charged particles we use either a count-rate curve in the Z channel or data from the 3DP instrument (Lin et al. 1995) located on the Wind spacecraft that provides information on the

fluxes of electrons in the 27–517 keV energy band and protons in the 71–6800 keV energy band. The total fraction of the Konus-Wind observation time contaminated by solar energetic particles is $\lesssim 8\%$; data obtained during these intervals are not included in the database.

Currently, the KW-Sun database contains light curves in the G1, G2, and G3 channels, multichannel spectra, and detector response matrices for the flares registered in the triggered mode. The data are described in the following sections and summarized in Table 1. A detailed data description is also available at the KW-Sun website.¹⁰ An example of a web interface to the data for a specific flare is given in Figure 4.

⁹ The GOES event list is available via <https://hesperia.gsfc.nasa.gov/goes/>.

¹⁰ <http://www.ioffe.ru/LEA/kwsun/kw-info.html>

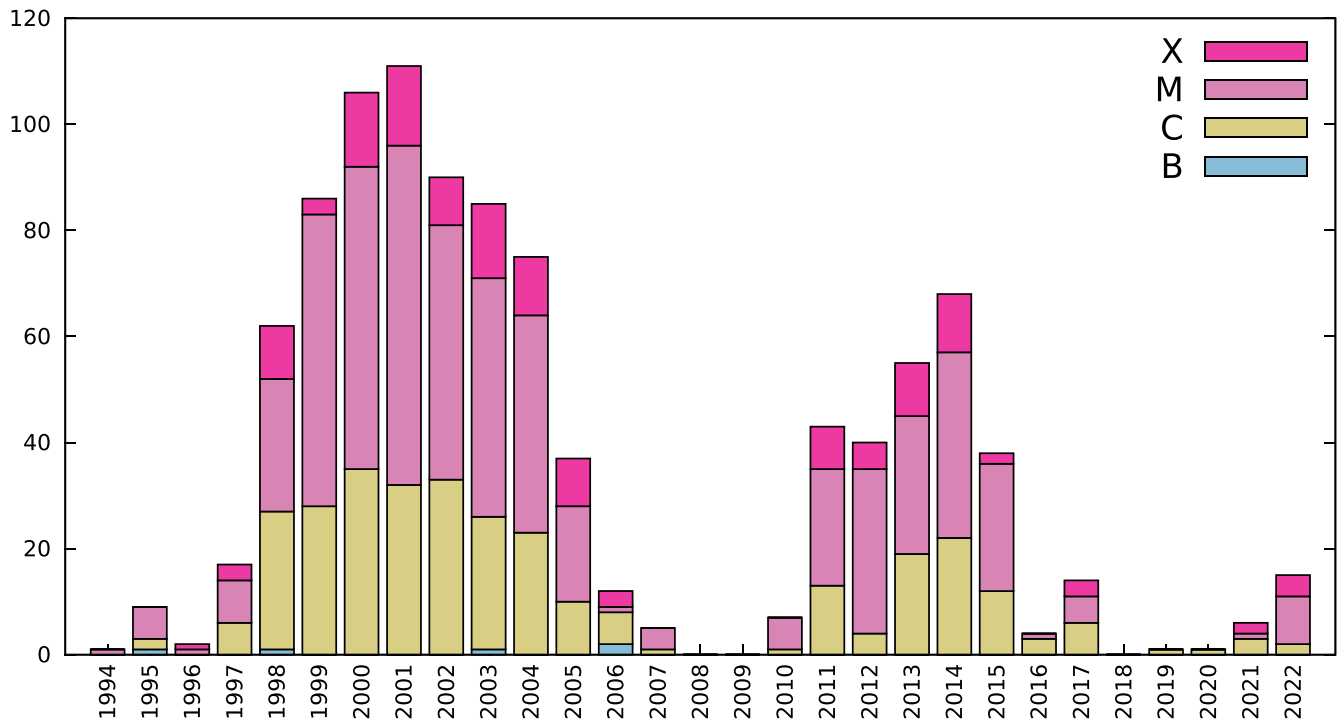


Figure 3. Annual rate of solar flares registered by Konus-Wind in the triggered mode categorized by the GOES classes.

Table 1
Data Types Presented in the KW-Sun Repository

Data Type	Energy Range	Time Resolution	Record Duration (s) ^a	Format
Light curves	Three channels: G1, G2, G3 ~20–1200 keV	16, 64, 256 ms ^b , 2.944 s ^c	~250	ASCII, IDL SAV
Multichannel spectra	First range: 63 channels, 20–1200 keV Second range: 60 channels, 350 keV–15 MeV	64 ms–8.192 s	≤492	FITS, OGIP standard PHA Type-II—spectral files PHA Type-I—background files RMF, ARF—response files

Notes,

^a After trigger time.

^b Triggered mode.

^c Waiting mode.

As Wind is located at distances up to ~ 6 lt-s from Earth, for every flare in addition to the Konus-Wind trigger time (UT) we provide the trigger time corrected for the light propagation time from Wind to the Earth’s center (geocenter time) in order to compare Konus-Wind observations with observations made by Earth-based or Earth-orbiting instruments. It should be noted that the geocenter times may differ from UT at near-Earth spacecraft or ground-based locations by up to ~ 20 ms.

3.1. Light Curves

Light curves in the KW-Sun database are available in two formats: ASCII and IDL SAV, named as KYYYYMMDD_TSSSS.txt and KYYYYMMDD_TSSSS.sav respectively, where YYYYYMMDD is the flare date and SSSSS is the trigger time in seconds (UT). The data description is available at the top of the ASCII file and in the “description” section of the SAV file.

For each flare, the description contains the Konus-Wind trigger time (t_{kw} variable in the IDL SAV file), the

corresponding geocenter time (t_{earth} variable in the IDL SAV file) and the calibrated energy boundaries of the G1, G2, and G3 channels ($channels$ variable in the IDL SAV file).

The light curve data are stored in 11 columns in the ASCII file and in four variables in the IDL SAV file: the start and end times of the time bin (columns $t1$ and $t2$ in the ASCII file and tkw variable in the IDL SAV), relative to the trigger time; DT-corrected count rates in G1, G2, and G3 (columns $G1$, $G2$, $G3$ in the ASCII file and lc variable in the IDL SAV file); the background-subtracted and DT-corrected count rates (columns $G1bgsb$, $G2bgsb$, $G3bgsb$ in the ASCII file and lc_bgsb variable in the IDL SAV file); and the count-rate uncertainties at the 1σ level (columns $eG1$, $eG2$, $eG3$ in the ASCII file and lc_err variable in the IDL SAV file). The time history stored in the database includes several hundred seconds of waiting-mode data measured before the trigger time, which, for gradually rising flares, cover the beginning of the event (see Table 1).

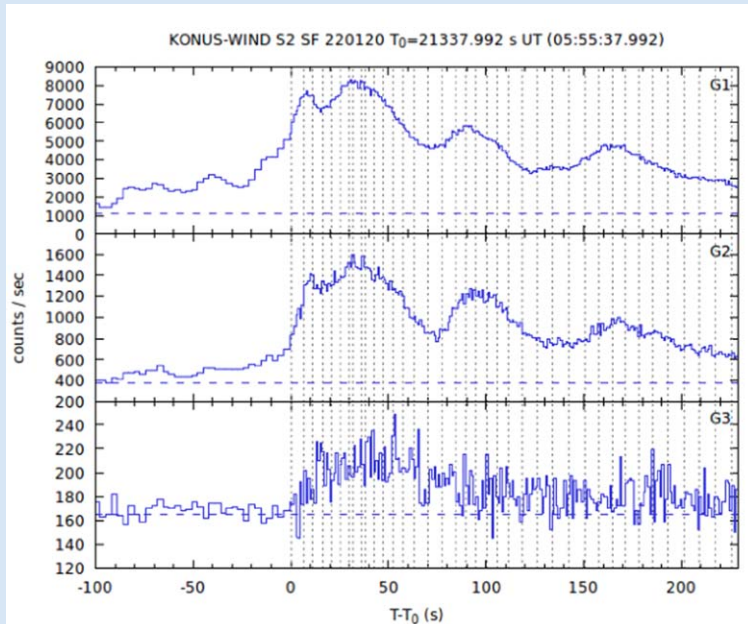
Konus-Wind occultations by other instruments and the spacecraft parts appear on millisecond timescales as dips in the light curves with a period of ~ 3 s. Figure 5 illustrates



Ioffe Institute. Laboratory for Experimental Astrophysics

KW-Sun: Konus-Wind Solar Flare Database

The flare on 20 January 2022, 05:55:37 (21337)



Konus-Wind X-ray light curves:

- [ASCII](#) – 3-ch light curve (ASCII format)
- [SAV](#) – 3-ch light curve (IDL SAV format)

Konus-Wind spectral data:

- [PHA-1](#) – low-energy spectral data
- [PHA-2](#) – high-energy spectral data
- [RMF-1](#) – low-energy response matrix
- [RMF-2](#) – high-energy response matrix
- [ARF](#) – auxiliary response file
- [BGPHA-1](#) – low-energy background data
- [BGPHA-2](#) – high-energy background data

[Data format description](#)

Page last updated: 20 Jun 2022

Figure 4. KW-Sun web interface to the data for a specific flare, which displays the flare light curves in G1, G2, G3 and provides links to the data. Horizontal dashed lines represent background levels, and vertical dotted lines in the plot indicate time intervals of multichannel spectrum accumulation.

occultation influence on solar flare time profiles. The total durations of the dips per rotation period constitute ~ 200 ms for S2 and ~ 600 ms for S1. The occultation positions are calculated based on the spacecraft spin-phase data, and the appropriate time intervals are removed from the light curves to ensure data reliability.

An example plot of the Konus-Wind time profile in G1, G2, and G3 is shown in Figure 4 for the M5.5 class flare of 2022 January 20.

3.2. Multichannel Energy Spectra

For each flare, KW-Sun provides multichannel energy spectra in the two energy ranges as PHA Type-II (PHA-II) FITS files, which contain multiple spectrum data sets. The corresponding background spectra (see below) are available as PHA Type-I (PHA-I) FITS files with a single data set. The spectra are complemented with detector response matrices (in RMF format) and an ancillary response file (in ARF format). All these data conform to OGIP specifications.¹¹ The detailed description of spectral and response files can be found in the [Appendix](#). The response matrices are calculated using the Geant4 toolkit (Agostinelli et al. 2003), for a parallel beam entering the detector at the incident angle of 90° to its axis. The

energy channel boundaries of the matrix are adjusted to match the appropriate detector calibration.

Spectra for the first energy range (~ 20 – 1200 keV) are measured by two redundant analyzers, PHA1 and PHA3. By default KW-Sun contains data from PHA1 (the FITS files are named as KWYYYYMMDD_TSSSSS_1.pha), but in the cases of data gaps in PHA1, we provide the data from PHA3 (files named as KWYYYYMMDD_TSSSSS_3.pha). Data for the second energy range (~ 0.35 – 15 MeV) are stored in files named as KWYYYYMMDD_TSSSSS_2.pha (see Table 1). Background spectrum files for the first energy range are named as KWYYYYMMDD_TSSSSS_1_bg.pha (or KWYYYYMMDD_TSSSSS_3_bg.pha if PHA3 is used, see above) and for the second energy range as KWYYYYMMDD_TSSSSS_2_bg.pha. Response matrices for the first energy range are named KWYYYYMMDD_TSSSSS_1.rmf (or KWYYYYMMDD_TSSSSS_3.rmf if PHA3 is used), for the second energy range KWYYYYMMDD_TSSSSS_2.rmf, and an ancillary response file is named as KWYYYYMMDD_TSSSSS.arf.

An example of the multichannel spectrum in the first (PHA1) and the second (PHA2) energy ranges is plotted in Figure 6 for the X9.3 class flare that occurred on 2017 September 6 and is described in Lysenko et al. (2019).

For most solar flares ($\sim 90\%$) data from the second, hard Konus-Wind energy range do not contain useful information on

¹¹ https://heasarc.gsfc.nasa.gov/docs/heasarc/ofwg/ofwg_intro.html

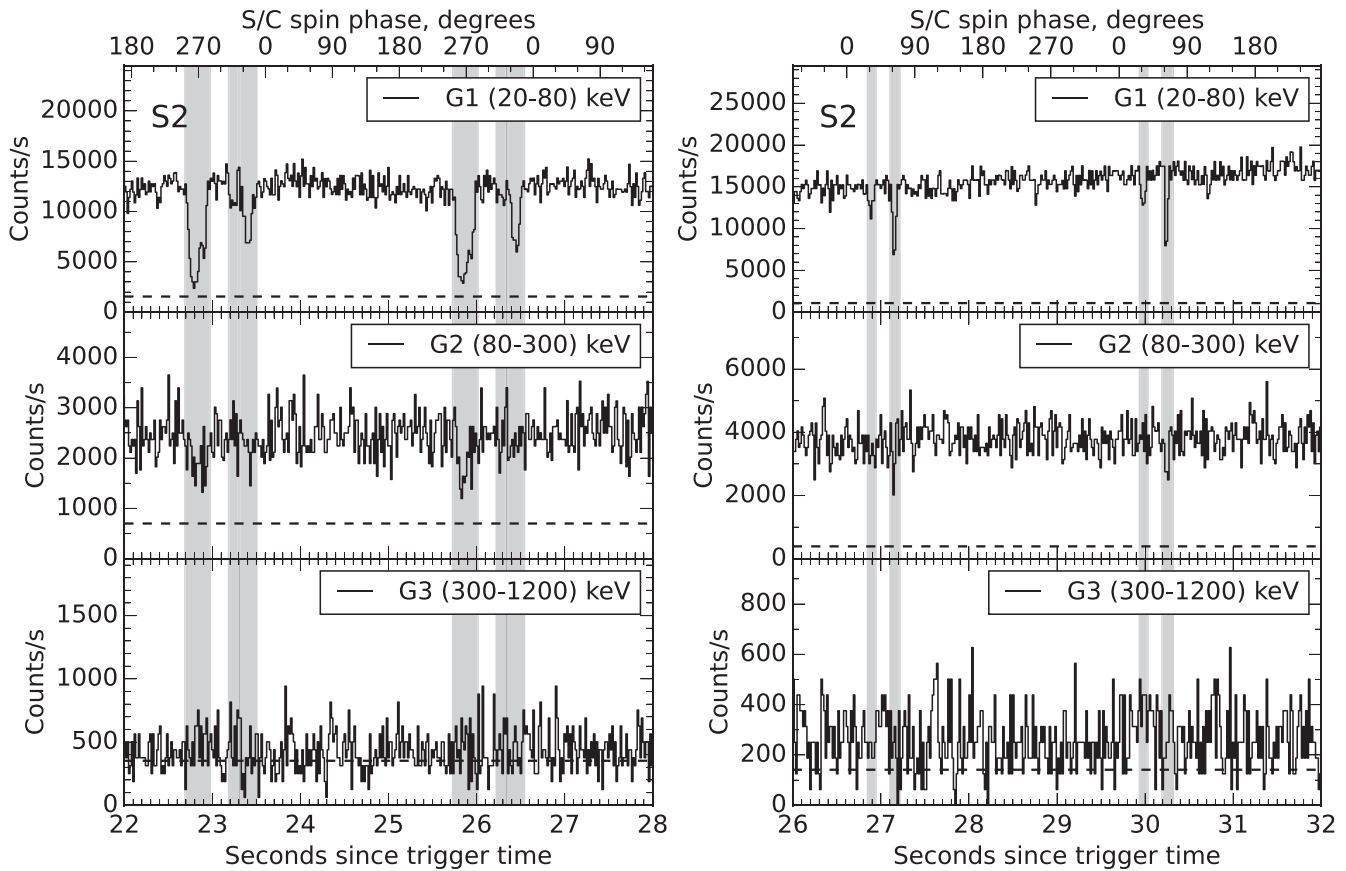


Figure 5. Occultations in the Konus-Wind solar flare time profiles for the S1 (left) and S2 (right) detectors. Gray shaded regions mark time intervals when the Sun was occulted partially or fully by other instruments or the spacecraft (S/C) structures. These intervals are removed from the KW-Sun light curves.

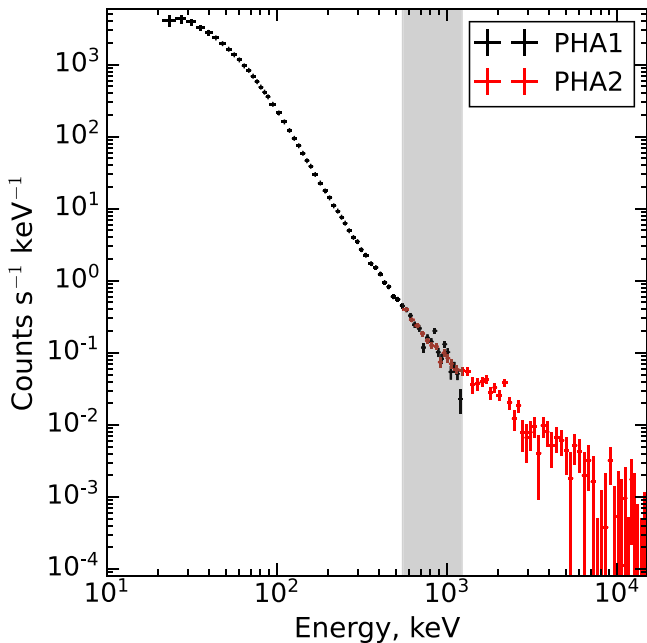


Figure 6. Example of a background-subtracted multichannel energy spectrum for the X9.3 class solar flare on 2017 September 6 in the first energy range (PHA1, black) and the second energy range (PHA2, red). The gray shaded area marks the PHA1/PHA2 overlapping range.

the emission. However, when data from both the first (PHA1 or PHA3) and second (PHA2) ranges are used in the analysis, it is necessary to exclude the spectral channels of the first band in

the overlapping range of energies (i.e., to ignore channels 42–63 of PHA1 or PHA3) due to two reasons. First, in this range PHA1 (PHA3) and PHA2 measure the signals produced by the same detected photons (yet the PHA2 low-energy discriminator is set at a 10× higher level), and second, for a typical steeply falling spectrum a smaller DT fraction in PHA2 leads to a better signal-to-noise ratio of the counts in the overlapping energy range (see Figure 6).

For short-duration solar flares, which end before the accumulation of the multichannel spectra has finished, the background spectra are selected as measured at the end of the trigger record. For the flares that last longer than the triggered record the background is taken from a nearby triggered event with similar background levels and close calibrations, and appropriate uncertainties are added in quadrature to the Poisson errors of the background counts (see the Appendix).

A table containing time intervals covered by multichannel spectra for all flares registered in the triggered mode is available online.¹²

The KW-Sun spectral data are suitable for analysis with standard tools for X-ray and gamma-ray spectral fitting, e.g., XSPEC (Arnaud 1996) and OSPEX (Schwartz et al. 2002; Tolbert & Schwartz 2020), the latter is part of the SOLARSOFT-WARE package. We provide a Unix utility SUMKONUSPECTRA¹³ that extracts (and merges, if needed) individual Konus-Wind spectra from the PHA-II format files, which contain multiple multichannel spectra, to PHA-I format files, which

¹² http://www.ioffe.ru/LEA/kwsun/KW_spectrum_times.txt

¹³ <http://www.ioffe.ru/LEA/kwsun/kw-info.html>

contain data on a single spectrum. We recommend using this utility when working with XSPEC. The OSPEX package accepts inputs in PHA-II and allows searching for flares in the KW-Sun database, downloading Konus-Wind spectral data automatically, and analyzing them using its common routines. Both XSPEC and OSPEX load appropriate background and response files automatically when a spectral PHA file is selected for the analysis.

3.3. Instrumental Effects at High Intensities

3.3.1. Integer Overflows in Low-energy Spectral Channels

At high incident photon fluxes, integer overflows in low-energy channels of PHA1 (PHA3) (≤ 40 keV) may occur that result in underestimation of the total count number, DT, and flux; and also in the spectrum distortion. We use a special algorithm for the overflow corrections, but, for some very intense flares, incorrect values in the first channels of PHA1 (PHA3) can appear anyway. Thus, in the cases of bad fit residuals in the low-energy channels, it is recommended to exclude these channels from the analysis.

3.3.2. Circuit Saturation and Pulse-pileup Effects

For intense events, the standard Konus-Wind DT correction procedure (see Section 2) results in flux underestimation due to saturations in the instrument's signal shaper and counter logic circuits. Such saturations are not negligible in PHA1 (PHA3) at incident photon rates per detector area n exceeding $\sim 2 \times 10^4$ photon s^{-1} , and in the G1, G2, and G3 channel counters at $n \gtrsim 2.5 \times 10^5$ photon s^{-1} . At considerably higher photon rates, the shape of the spectrum can also be distorted due to the pulse-pileup effect. We studied the influence of the pileup effect using Monte Carlo modeling and found that it becomes significant for PHA1 (PHA3) at $n \gtrsim 5 \times 10^4$ photon s^{-1} .¹⁴

For the events of moderate intensity (2×10^4 photon $s^{-1} < n < 5 \times 10^4$ photon s^{-1} , $\sim 15\%$ of all triggered flares) the flux in PHA1 (PHA3) can be underestimated, but this uncertainty does not exceed $\sim 10\%$, thus no additional corrections are needed. For high-intensity events ($n > 5 \times 10^4$ photon s^{-1} , $\sim 8\%$ of all triggered flares) the corrections are applied for both spectral shape and flux. In practice, the saturation correction to PHA1 (PHA3) count rate can be estimated using DT-corrected counts in the overlapping PHA1/PHA2 energy range (see Section 3.2). For the cases of additional DT corrections applied for high-intensity flares two columns with count and exposure uncertainties are added to the PHA files. These systematic errors are taken into account automatically both in XSPEC and OSPEX (see the Appendix). As the pileup correction procedure is time consuming, corrected PHA1 (PHA3) data are available only for a subset of intense flares, while for other flares spectral data for the first energy range are not available from the database and the appropriate note is added to the web page of the flare. In the latter case, we encourage the user to contact the KW-Sun team by e-mail for pileup-corrected spectra of the event they are interested in.

¹⁴ The detailed description of pileup corrections for Konus-Wind data is given in the Appendix of Lysenko et al. (2019).

3.3.3. Uncertainties with Energy Calibration

One more issue for high-intensity events is the calibration uncertainties resulting from the fact that the lines used in the calibration are faintly distinguishable above the continuum. Although these uncertainties do not exceed a few percent, they may be important in the gamma-ray emission-line studies.

4. Summary and Conclusion

In this paper, we presented KW-Sun—the online catalog of solar flares registered by the Konus-Wind experiment in hard X-ray and soft gamma-ray ranges during more than two full solar cycles. The database contains light curves with high (down to 16 ms) time resolution and multichannel spectra in the wide-energy range (~ 20 keV–15 MeV) for more than 1000 solar flares detected by the instrument in the triggered mode.

The main area of application of the Konus-Wind data for solar physics is the study of the emission from accelerated electrons and ions. The high time resolution in the triggered mode allows for the examination of properties of nonthermal electrons on subsecond timescales, which is crucial for the research of the acceleration mechanisms during magnetic reconnection. Other advantages of Konus-Wind for solar flare studies are the absence of the Earth's occultations and extremely stable background conditions due to its location in interplanetary space. The presented homogeneous data set can be used for both statistical and case studies of solar flares. Now with the beginning of a new solar cycle, this may be especially in demand as there is no solar-dedicated instrument in hard X-ray range near the Earth.

KW-Sun database is a work in progress and data on new flares are added as they become available. The major “to-do task” is to extend KW-Sun with numerous solar flares registered in the waiting mode and to provide response matrices for three-channel time-history data, which will allow spectral fitting of Konus-Wind G1, G2, and G3 data with simple spectral models at fine timescales. Future enhancements of KW-Sun will be available via the database website at Ioffe.¹⁵

We thank Prof. A. K. Tolbert for her help with incorporating Konus-Wind data in OSPEX package. A.A.K. and L.K.K. were supported by the Ministry of Science and Higher Education of the Russian Federation. G.D.F. was supported in part by NSF grant AGS-2121632 and NASA grant 80NSSC19K0068 to New Jersey Institute of Technology.

Appendix

Structure of FITS Files in OGIP Standard




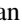

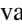

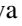
PHA-II files contain the EBOUNDS extension with boundaries of energy channels (columns E_MIN and E_MAX) and the SPECTRUM extension that includes the start (column TSTART), stop (column TSTOP), and exposure (column EXPOSURE) time of spectrum accumulation and $N_{sp} \times N_{ch}$ matrix (COUNTS) with the count number in each of N_{ch} channels for $N_{sp} = 64$ multichannel spectra. The separate file with background multichannel spectra in PHA-I format contains the EBOUNDS extension with energy boundaries equal to those of a flare spectrum and a single spectrum in the SPECTRUM extension with columns CHANNEL, RATE, STAT_ERR, SYS_ERR, GROUPING, and QUALITY.

¹⁵ <http://www.ioffe.ru/LEA/kwsun/>

Standard Konus-Wind DT corrections (Section 2) are taken into account in the EXPOSURE column for PHA-II files and in the RATE and STAT_ERR columns of PHA-I files. Systematic errors associated with additional DT corrections for very intense events (see Section 3.3.2) are added in quadrature to the statistical errors in each channel, and the resulting errors are written to the STAT_ERR column in the PHA files. This column (if it exists) is automatically used by XSPEC and OSPEX instead of Poisson errors for count spectra. Exposure errors caused by these corrections are added, for the information, to the EXPOSURE_ERR column in the PHA file.

RMF files consist of the EBOUNDS and MATRIX extensions. MATRIX includes columns ENERG_LO and ENERG_HI with $N_i = 263$ incident energies E_i of test quanta used for response modeling and an $N_i \times N_{\text{ch}}$ matrix with the probabilities of registering a gamma-quantum of energy E_i in channel N_i compressed by a special algorithm.¹⁶ ARF files contain the SPECRESP extension with effective areas calculated for $N_i = 263$ incident energies E_i of test quanta.

ORCID iDs

A. L. Lysenko  <https://orcid.org/0000-0002-3942-8341>
M. V. Ulanov  <https://orcid.org/0000-0002-0076-5228>
A. A. Kuznetsov  <https://orcid.org/0000-0001-8644-8372>
G. D. Fleishman  <https://orcid.org/0000-0001-5557-2100>
D. D. Frederiks  <https://orcid.org/0000-0002-1153-6340>
L. K. Kashapova  <https://orcid.org/0000-0003-2074-5213>
D. S. Svinkin  <https://orcid.org/0000-0002-2208-2196>
A. E. Tsvetkova  <https://orcid.org/0000-0003-0292-6221>

References

Acton, L., Bruner, M., Lemen, J., et al. 1992, *Sci*, 258, 618

- Agostinelli, S., Allison, J., Amako, K., et al. 2003, *NIMPA*, 506, 250
Ajello, M., Baldini, L., Bastieri, D., et al. 2021, *ApJS*, 252, 13
Altyntsev, A. T., Meshalkina, N. S., Lysenko, A. L., & Fleishman, G. D. 2019, *ApJ*, 883, 38
Aptekar, R. L., Frederiks, D. D., Golenetskii, S. V., et al. 1995, *SSRv*, 71, 265
Arnaud, K. A. 1996, in ASP Conf. Ser. 101, *Astronomical Data Analysis Software and Systems V*, ed. G. H. Jacoby & J. Barnes (San Francisco, CA: ASP), 17
Atwood, W. B., Abdo, A. A., Ackermann, M., et al. 2009, *ApJ*, 697, 1071
Crosby, N. B., Aschwanden, M. J., & Dennis, B. R. 1993, *SoPh*, 143, 275
Dennis, B. R. 1985, *SoPh*, 100, 465
Emslie, A. G., Dennis, B. R., Shih, A. Y., et al. 2012, *ApJ*, 759, 71
Fleishman, G. D., Nita, G. M., Chen, B., Yu, S., & Gary, D. E. 2022, *Natur*, 606, 674
Fletcher, L., Dennis, B. R., Hudson, H. S., et al. 2011, *SSRv*, 159, 19
Glesener, L., & Fleishman, G. D. 2018, *ApJ*, 867, 84
Hannah, I. G., Christe, S., Krucker, S., et al. 2008, *ApJ*, 677, 704
Holman, G. D., Aschwanden, M. J., Aurass, H., et al. 2011, *SSRv*, 159, 107
Krucker, S., Hurford, G. J., Grimm, O., et al. 2020, *A&A*, 642, A15
Lin, R. P., Anderson, K. A., Ashford, S., et al. 1995, *SSRv*, 71, 125
Lin, R. P., Dennis, B. R., Hurford, G. J., et al. 2002, *SoPh*, 210, 3
Lysenko, A. L., Anfinogentov, S. A., Svinkin, D. S., Frederiks, D. D., & Fleishman, G. D. 2019, *ApJ*, 877, 145
Lysenko, A. L., Frederiks, D. D., Fleishman, G. D., et al. 2020, *PhyU*, 63, 818
Meegan, C., Lichti, G., Bhat, P. N., et al. 2009, *ApJ*, 702, 791
Müller, D., St., Cyr, O. C., Zouganelis, I., et al. 2020, *A&A*, 642, A1
Ogawara, Y., Takano, T., Kato, T., et al. 1991, *SoPh*, 136, 1
Schwartz, R. A., Csillaghy, A., Tolbert, A. K., et al. 2002, *SoPh*, 210, 165
Share, G. H., Murphy, R. J., White, S. M., et al. 2018, *ApJ*, 869, 182
Svinkin, D. S., Frederiks, D. D., Aptekar, R. L., et al. 2016, *ApJS*, 224, 10
Tolbert, K., & Schwartz, R. 2020, OSPEX: Object Spectral Executive, Astrophysics Source Code Library, ascl:2007.018
Vestrand, W. T., Share, G. H., J. Murphy, R., et al. 1999, *ApJS*, 120, 409
Vilmer, N., MacKinnon, A. L., & Hurford, G. J. 2011, *SSRv*, 159, 167
Wilson, L. B. I., Brosius, A. L., Gopalswamy, N., et al. 2021, *RvGeo*, 59, e2020RG000714

¹⁶ Response matrix compression is described in OGIP standard.